The Jumonji-C oxygenase JMJD7 catalyzes (3S)-lysyl hydroxylation of TRAFAC GTPases

Markolovic, Suzana; Zhuang, Qinqin; Wilkins, Sarah E. ; Eaton, Charlotte; Abboud, Martine I. ; Katz, Maximiliano J. ; McNeil, Helen; Leśniak, Robert K. ; Hall, Charlotte; Struwe, Weston B. ; Konietzny, Rebecca ; Davis, Simon ; Yang, Ming ; Ge, Wei; Benesch, Justin L P ; Kessler, Benedikt M. ; Ratcliffe, Peter J. ; Cockman, Matthew E. ; Fischer, Roman ; Wappner, Pablo

DOI:
10.1038/s41589-018-0071-y

Document Version
Peer reviewed version

Citation for published version (Harvard):
Markolovic, S, Zhuang, Q, Wilkins, SE, Eaton, C, Abboud, MI, Katz, MJ, McNeil, H, Leśniak, RK, Hall, C, Struwe, WB, Konietzny, R, Davis, S, Yang, M, Ge, W, Benesch, JLP, Kessler, BM, Ratcliffe, PJ, Cockman, ME, Fischer, R, Wappner, P, Chowdhury, R, Coleman, M & Schofield, CJ 2018, 'The Jumonji-C oxygenase JMJD7 catalyzes (3S)-lysyl hydroxylation of TRAFAC GTPases', *Nature Chemical Biology*, vol. 14, no. 7, pp. 688-695. https://doi.org/10.1038/s41589-018-0071-y

Europe PMC Funders Author Manuscripts

The Jumonji-C oxygenase JMJD7 catalyzes (3*S*)-lysyl hydroxylation of TRAFAC GTPases

Suzana Markolovic[1,7], **Qinqin Zhuang**[2,7], **Sarah E Wilkins**[1,8], **Charlotte D Eaton**[2,8], **Martine I Abboud**[1,8], **Maximiliano J Katz**[3,8], **Helen E McNeil**[2], **Robert K Leśniak**[1], **Charlotte Hall**[2], **Weston B Struwe**[1], **Rebecca Konietzny**[4], **Simon Davis**[4], **Ming Yang**[4,5], **Wei Ge**[1], **Justin LP Benesch**[1], **Benedikt M Kessler**[4], **Peter J Ratcliffe**[4,5], **Matthew E Cockman**[4,5], **Roman Fischer**[4], **Pablo Wappner**[3], **Rasheduzzaman Chowdhury**[1,6,*], **Mathew L Coleman**[2,9,*], and **Christopher J Schofield**[1,9,*]

[1]Chemistry Research Laboratory, Department of Chemistry, University of Oxford, Oxford, United Kingdom

[2]Institute of Cancer and Genomic Sciences, University of Birmingham, Birmingham, United Kingdom

[3]Instituto Leloir, Buenos Aires, Argentina

[4]Target Discovery Institute, University of Oxford, Oxford, United Kingdom

[5]The Francis Crick Institute, London, United Kingdom

Abstract

[*]To whom correspondence should be addressed. rasheduzzaman.chowdhury@stanford.edu, m.coleman@bham.ac.uk, christopher.schofield@chem.ox.ac.uk.
[6]Present address: Stanford University School of Medicine, Department of Molecular and Cellular Physiology, Clark Center, Stanford, CA, USA.
[7,8,9]These authors contributed equally to this work.

Author Contributions

S.M., Q.Z., S.E.W., M.J.K., P.W., R.C., M.L.C, and C.J.S. designed and conceived the research; S.M. prepared recombinant proteins; Q.Z. performed substrate discovery proteomics; S.M. performed and analyzed CD spectra and all enzyme activity assays by MALDI-MS and NMR; Q.Z. performed enzyme:substrate interaction assays; S.M. and R.C. performed the crystallography in which R.C. played both an experimental and supervisory role; C.E. performed confocal microscopy, cellular dimerization, and dmJMJD7 interaction experiments; Q.Z., C.H., and H.E.M. prepared mammalian expression constructs used by Q.Z.; W.G. and S.M. prepared plasmids for recombinant protein production; S.M. performed / analyzed amino acid analyses with guidance from S.E.W; M.I.A. performed and analyzed peptide NMR work; Q.Z. purified exogenous and endogenous proteins for MS / analyzed data with help from M.L.C; M.I.A. produced and purified recombinant DRG1, performed DRG1 stability and activity assays, and analyzed data; R.K., S.D., and R.F. performed MS (B.M.K.) and analyzed data; Q.Z. performed all JMJD7 loss-of-function experiments and DRG/DFRP interaction, GTPase, and RNA binding assays; R.K.L. prepared hydroxylysine standards; S.M. and W.B.S. performed and analyzed native MS / SEC-MALS (J.L.B.); M.J.K. and P.W. performed and analyzed *Drosophila* experiments; R.C. performed enzyme:substrate modelling, prepared recombinant dmJMJD7, and performed proteolysis assays; M.Y., M.E.C., and P.J.R. performed preliminary immunoprecipitations; S.M., Q.Z., S.E.W., C.E., R.C., M.L.C., and C.J.S. analyzed data; S.M., Q.Z., R.C., M.L.C., and C.J.S. wrote the manuscript.

Competing Interests

The authors declare no competing interests.

Data availability

Atomic coordinates and structure factors for crystal structures have been deposited in the Protein Data Bank under the accession codes: 5NFN and 5NFO. Mass Spectrometry data are available under PXD009263 at www.proteomexchange.org/.

Biochemical, structural, and cellular studies reveal Jumonji-C (JmjC) domain-containing 7 (JMJD7) as a 2-oxoglutarate (2OG)-dependent oxygenase catalyzing a previously unreported type of post-translational modification, (*3S*)-lysyl hydroxylation. Crystallographic analyses reveal JMJD7 as more closely related to the JmjC hydroxylases rather than the JmjC demethylases. Biophysical and mutation studies show that JMJD7 has a unique dimerization mode, with interactions between monomers involving both *N*- and *C*-terminal regions and disulfide bond formation. A proteomic approach identifies two related members of the Translation Factor (TRAFAC) family of GTPases, Developmentally Regulated GTP Binding Proteins 1 and 2 (DRG1/2), as activity-dependent JMJD7 interactors. Mass spectrometric analyses demonstrate that JMJD7 catalyzes Fe(II)- and 2OG-dependent hydroxylation of a highly-conserved lysine residue in DRG1/2; amino acid analyses reveal JMJD7 catalyzes (3*S*)-lysyl hydroxylation. The functional assignment of JMJD7 will enable future studies to define the role of DRG hydroxylation in cell growth and disease.

Introduction

Following their initial identification as pro-collagen prolyl and lysyl hydroxylases, Fe(II) and 2-oxoglutarate (2OG)-dependent oxygenases have emerged as widespread regulators of protein biosynthesis[1,2]. The hypoxia inducible factor prolyl- and asparaginyl- hydroxylases regulate the levels and transcriptional activity of the αβ-hypoxia inducible transcription factors (HIFs). Prolyl hydroxylation, by the prolyl hydroxylase domain (PHDs/EGLNs) oxygenases, regulates HIF-α subunit levels by signaling for degradation, while asparaginyl hydroxylation (catalyzed by Factor inhibiting hypoxia inducible factor, FIH) regulates HIF transcriptional activity; the sensitivity of the PHDs and FIH catalysis to cellular oxygen availability enable them to act as hypoxia sensors[3]. FIH, but not the PHDs, is a member of the Jumonji-C (JmjC) subfamily of 2OG oxygenases[4], other members of which regulate transcription via demethylation of the three histone lysine N^{ε}-methylation states. JmjC histone demethylase (KDM) catalysis proceeds via hydroxylation to give a hemiaminal intermediate, which fragments to give the demethylated product and formaldehyde[5]. There are ~6 human JmjC KDM subfamilies, which are being studied due to their roles in transcription and links to cancer and genetic disorders resulting from mutations to them[6]. 2OG oxygenases are current therapeutic targets with compounds being developed for clinical applications in cancer (e.g. KDM5 inhibitors)[7] and anemia (PHD inhibitors)[8].

With the exception of FIH, there are limited reports on the ~10 human JmjC oxygenases that catalyze formation of stable alcohol products ('JmjC hydroxylases'), which are less well-studied than the JmjC KDMs. In addition to HIF-α isoforms, FIH catalyzes modification of ankyrin repeat domains[9], and Jumonji domain-containing 6 (JMJD6) catalyzes hydroxylation of splicing regulatory proteins[10]. JmjC hydroxylases also have ancient roles in regulation of protein biosynthesis by modifying the translational machinery[11]. The ribosomal oxygenases (RiOX), MYC-induced nuclear antigen (MINA53) and nucleolar protein 66 (NO66) catalyze histidinyl hydroxylation of Rpl27a and Rpl8, respectively[12]. tRNA yW-synthesizing enzyme 5 (TYW5) is a tRNA hydroxylase[13], and Jumonji domain-containing 4 (JMJD4) catalyzes hydroxylation of eukaryotic release factor 1 (eRF1), a reaction increasing stop codon recognition efficiency[14]. In eukaryotes ranging from yeasts

to humans, a 2OG oxygenase that is not a JmjC protein (human: OGFOD1; *Drosophil*a: Sudestada1), but which is related to the HIF PHDs, catalyzes hydroxylation of a prolyl residue in close contact with mRNA in ribosomes15. Overall, these results indicate that multiple 2OG oxygenases are involved in regulation of protein synthesis at both transcriptional and translational levels2,15.

Jumonji domain-containing 7 (JMJD7) is one of the few remaining biochemically uncharacterized human JmjC oxygenases; structure-based bioinformatics predicts it is an Fe(II) and 2OG-dependent oxygenase containing a JmjC catalytic domain (Supplementary Fig. 1). We report biochemical, crystallographic, and cellular studies revealing JMJD7 as a structurally distinct JmjC hydroxylase catalyzing a previously unreported post-translational modification (PTM), (3*S*)-lysyl hydroxylation, in two related members of the Translation Factor (TRAFAC) GTPase family. The results will enable future work to elucidate the biological roles of JMJD7 in protein synthesis, the regulation of cell growth, and disease.

Results

JMJD7 suppresses cell growth in Drosophila

In an RNAi-based screen for variations in size of the *Drosophila* posterior wing compartment, we observed that knockdown of CG10133 mRNA, the *Drosophila* orthologue of human JMJD7 (dmJMJD7, 45% sequence identity), correlates with increased posterior wing compartment size, likely through an increase in cell size (Supplementary Fig. 2). Among human JmjC proteins, structure-based bioinformatics predicts JMJD7 is most closely related to FIH4, TYW513, Jumonji domain-containing 5 (JMJD5)16, and the RiOXs, MINA53 and NO6611, all of which are JmjC hydroxylases with roles in protein biosynthesis regulation (in some cases, they are also reported to have KDM activities). Because the catalytic activities and structures of the JmjC oxygenases can relate to their physiological roles17, we undertook biochemical studies on JMJD7.

JMJD7 is structurally similar to JmjC hydroxylases

Analysis of the activity of recombinant JMJD7 using ^{1}H NMR reveals slow Fe(II)-stimulated conversion of 2OG to succinate in the absence of a substrate (Supplementary Fig. 3). As observed for some other 2OG oxygenases, this conversion was reduced by the broad spectrum inhibitor, *N*-oxalylglycine (NOG)18; alanine substitution of one of the predicted Fe(II)-binding residues (H178) also reduces 2OG turnover (Supplementary Figs. 1 and 3b-c). To support biochemical characterization of JMJD7 and to investigate whether it functions as a hydroxylase and/or KDM, we then worked to solve crystal structures for human JMJD7.

A structure of full-length His_6-tagged JMJD7 complexed with 2OG and Mn(II), an inert Fe(II) substitute, was solved by molecular replacement (Fig. 1). We obtained a higher resolution (2.2 Å) structure of a JMJD7 variant arising from a missense mutation (R260C) present in endometrial cancer19 and autism20 (Supplementary Fig. 1), the fold of which is very similar to wildtype (0.35 Å Cα root mean squared deviation; Supplementary Fig. 4 and Supplementary Table 1). JMJD7 crystallizes as an oligomer with two or four molecules in each asymmetric unit (Fig. 1 and Supplementary Fig. 4). Biophysical analyses reveal JMJD7 as dimeric in solution, consistent with immunoprecipitation studies in cells (Supplementary

Fig. 5a-c). Uniquely among characterized JmjC proteins, JMJD7 dimerization involves hydrophobic interactions between α-helices from *both N*- and *C*-terminal regions (α1, α2, and α9, respectively) and a disulfide involving Cys-47 from two monomers (Fig. 1a; Supplementary Figs 5d-e and 6). The dimeric state of JMJD7 suggests a closer structural similarity to the JmjC hydroxylases, rather than the demethylases17, since the former are commonly observed as dimers: FIH21 and TYW513 oligomerize via *C*-terminal α-helical bundles, while MINA53 and NO66 oligomerize via α-helical bundles located between their JmjC and winged-helix domains11 (Supplementary Fig. 5e).

The structures reveal each JMJD7 molecule is comprised of 9 α-helices, 18 β-strands, and 2-3_{10} helices. The catalytic domain contains the characteristic 2OG oxygenase distorted double-stranded β-helix (DSBH) core barrel, formed from 8 β-strands, arranged as 2 antiparallel major (βI, βVIII, βIII, βVI) and minor (βII, βVII, βIV, βV) sheets17. The DSBH houses the active site, where the 2OG oxalyl group, water, and the metal-binding triad (H178, D180, and H277) coordinate the metal in an octahedral geometry (Fig. 1b). The 2OG C1 carboxylate is positioned to make a hydrogen bonding network with the amides of N184 and N289. As with most structurally characterized JmjC oxygenases, the 2OG C5 carboxylate interacts via electrostatic and hydrogen bonding interactions with a lysine (K193) on βIV17. Most 2OG oxygenases have 2 or 3 polar side-chains positioned to interact with the 2OG C5 carboxylate group; notably, JMJD7 has 4 such side-chains. In addition to K193, the hydroxyls of Y127, T175, and Y186 form additional hydrogen bonds with the 2OG C5 carboxylate group (Fig. 1b). The apparently tight binding of 2OG is consistent with the observed slow substrate uncoupled 2OG turnover (Supplementary Fig. 3).

Comparison of the JMJD7 active site with those of other JmjC oxygenases reveals closer structural similarity with JmjC hydroxylases than KDMs. Notably, binding of the 2OG C1 carboxylate, involving hydrogen bonds with the N184 and N289 side-chain amides, emulates interactions made by FIH4, i.e. with the $N205_{FIH}$ and $N294_{FIH}$ side-chains (Supplementary Fig. 7a). Importantly, JMJD7 lacks a hydrophobic region crucial in binding the N^{ε}-methyl lysine group of the JmjC KDMs17. Most JmjC KDMs tend to have an extended loop at the *N*-terminus of DSBH βI that is involved in substrate binding; this is shortened in JMJD7 as in other JmjC hydroxylases (Supplementary Fig. 7b)17. Consistent with the absence of structural domains associated with KDM activity (e.g. characteristic histone- and nucleic acid-binding domains; Supplementary Fig. 7c), a panel of histone H3.1 fragments known to be JmjC KDM substrates were not modified by JMJD7 (Supplementary Fig. 8). Overall, the combined biophysical analyses reveal JMJD7 as having greater structural similarity to the JmjC hydroxylases than the JmjC KDMs.

Proteomics identifies TRAFAC GTPases as JMJD7 interactors

To identify potential JMJD7 substrates, we used mass spectrometry (MS) to compare the proteins interacting with wildtype and (near) inactive (H178A) JMJD7, using dimethyl-*N*-oxalylglycine (DMOG), a cell-penetrating precursor of NOG14, to trap substrates. Immunoaffinity purifications from extracts of DMOG-treated cells expressing FLAG-tagged wildtype or JMJD7 H178A were analyzed. JMJD7-specific interactions ablated by the H178A mutation included two closely related GTPases, Developmentally Regulated GTP

Binding Proteins 1 and 2 (DRG1/2), and their respective binding partners, DRG family regulatory proteins 1 and 2 (DFRP1/2) (Fig. 2a and Supplementary Fig. 9a)22. Known JmjC hydroxylase substrates (e.g. eRF1, splicing factors, HIFα, Rpl27a/Rpl8), ankyrins, or KDM substrates (e.g. histones) were not detected. Activity-dependent interactions of JMJD7 with DRG1 and DRG2 were confirmed in different cell lines (Supplementary Fig. 9b-d). Reciprocal immunoprecipitations using FLAG-tagged DRGs confirmed the interaction with endogenous JMJD7, but not the related hydroxylase JMJD4 (Supplementary Fig. 9e). Importantly, purification of endogenous DRG/DFRP complexes also co-precipitated endogenous JMJD7 (but not JMJD4; Fig. 2b). To investigate whether JMJD7 and DRG1/2 co-localize, immunofluorescence staining of co-expressed JMJD7 and DRG1 or DRG2 was performed in HeLa cells (Fig. 2c). Consistent with the proteomic and co-immunoprecipitation data, we observed significant co-localization of JMJD7 with DRG1 and DRG2 in both nuclear and cytoplasmic compartments. Overall, the combined interaction and localization data support the assignment of DRG1 and DRG2 as JMJD7 interactors and potential substrates.

JMJD7 catalyzes DRG lysyl hydroxylation

To investigate whether DRG/DFRP complexes are JMJD7 substrates, HA-DRG1/2 and V5-DFRP1/2 were purified from cells overproducing control or FLAG-JMJD7, hydrolyzed by trypsin, then analyzed by MS. The results identified a single lysyl hydroxylation site in a highly conserved region in both DRG1 and DRG2, i.e. at K22/K21, respectively (Fig. 3a-b and Supplementary Fig. 10). Notably, in cells overexpressing JMJD7, we reproducibly observed increases in hydroxylated peptides corresponding to a ‘missed’ trypsin cleavage site in DRG1 (NK(OH)ATAHHLGLLK) and DRG2 (NK(OH)ATEYHLGLLK), suggesting that JMJD7-catalyzed hydroxylation hinders trypsin-catalyzed hydrolysis (Fig. 3b).

We then tested the cellular assignment of JMJD7-mediated DRG1/2 lysyl hydroxylation by assaying 20-mer peptide fragments spanning the DRG1 sequence as substrates (Supplementary Table 2; a 25-mer peptide, $DRG1_{16\text{-}40}$, was also used for biochemical characterization as described later in the text). Consistent with the cell results (Fig. 3a-b and Supplementary Fig. 9), the only peptide undergoing a JMJD7-dependent +16 Da shift was $DRG1_{21\text{-}40}$ (NKATAHHLGLLKARLAKLRR-NH_2; Fig. 3c). Peptide hydroxylation was impaired by the absence of 2OG and Fe(II) and inhibited by NOG18 or use of a JMJD7 H178A variant (Fig. 3d). Incubation under $^{18}O_2$ revealed that JMJD7 catalyzes incorporation of ^{18}O into its product, as observed for other 2OG protein hydroxylases (Supplementary Fig. 11). Alanine substitution at the hydroxylation site prevented hydroxylation and blocked interaction between isolated JMJD7 and DRG1/2 (Supplementary Figs. 12 and 13). Interestingly, the DRG-hydroxylation sites are highly conversed in almost all animals including *Drosophila* (Fig. 3a). Recombinant dmJMJD7 hydroxylates human DRG1 and 2 peptides with similar efficiency as human JMJD7 (Supplementary Fig. 14a, compare to Supplementary Fig. 15). Furthermore, dmJMJD7 is able to reconstitute activity-dependent interactions with endogenous DRG1 and DRG2 in human cells (Supplementary Fig. 14b). These analyses suggest JMJD7-catalyzed DRG hydroxylation is highly conserved in animals, possibly in a manner linked to the growth phenotype observed on *dmJMJD7* knockdown in *Drosophila* (Supplementary Fig. 2).

The DRG2 peptide ($DRG2_{20-39}$; NKATEYHLGLLKAKLAKYRA-NH_2) was a less efficient substrate than the analogous $DRG1_{21-40}$ substrate (Supplementary Fig. 15a-b). A structure of the DRG1 homologue from *Saccharomyces cerevisiae* [Ribosome-interacting GTPase 1 (RBG1), 66% sequence identity, PDB ID: 4A9A] reveals the K22 side-chain protrudes from a loop on a highly conserved region of a helix-turn-helix (HTH) motif (Fig. 3a and Supplementary Fig. 15c)23. Strikingly, the position of K22 in the HTH of RBG1, and by implication DRG1/2, resembles that of the lysyl hydroxylation site of a JMJD4 substrate, eRF114 (Supplementary Fig. 15c-d). The location of K22 protruding from a turn between 2 α-helices suggests secondary structure may be important in JMJD7-substrate recognition, as for JMJD414. Increasing the DRG1 fragment length at its *N*-terminus to include other conserved residues in the HTH ($DRG1_{16-40}$; *ARTQK*NKATAHHLGLLKARLAKLRR-NH_2) results in more efficient hydroxylation (Supplementary Fig. 15a-b). Importantly, the *N*-terminally extended $DRG2_{15-39}$ fragment (*ARTQK*NKATEYHLGLLKAKLAKYRA-NH_2) undergoes efficient hydroxylation. To investigate how JMJD7 interacts with DRG1/2, we attempted to obtain JMJD7.DRG1/2 crystal structures, but have as yet been unsuccessful. We therefore modelled JMJD7.Fe.2OG.DRG1 complexes based on the crystal structures of JMJD7.Mn.2OG (PDB: 5NFO) and *S. cerevisiae* RBG1 (PDB: 4A9A). The modelling and cysteine substitution studies (Supplementary Fig. 16) support the combined biochemical observations implying long-range interactions involving conserved residues distant from those immediately surrounding the hydroxylated lysine are important in productive JMJD7 binding. Overall, the combined cellular and isolated protein studies define JMJD7 as a lysyl hydroxylase acting on both DRG1 and DRG2.

To investigate whether JMJD7 is *necessary* for hydroxylation of DRGs, we immunopurified endogenous DRG1/2 from HEK293T cells (Supplementary Fig. 17); MS analyses identified substantial levels of both K22 (Supplementary Fig. 17d) and K21 (Fig. 3e-f) hydroxylation, respectively. Importantly, endogenous levels of DRG2 K21 hydroxylation depended on the presence of JMJD7 expression (Fig. 3f and Supplementary Fig. 17b). Consistent with the overexpression analyses (Fig. 3b and Supplementary Fig. 10), the ability of trypsin to cleave endogenous DRGs at the *C*-terminal side of K22/K21 was reduced following hydroxylation (Fig. 3f). We also observed inhibition of DRG hydrolysis by hydroxylation with Lys-N, which cleaves at the *N*-terminal side of lysyl-residues (Supplementary Fig. 18). This phenomenon has not been reported following hydroxylation of lysine at the C4 or C5 positions by protein hydroxylases14,24,25, implying JMJD7 catalyzes a novel form of lysyl hydroxylation.

JMJD7 is a (3*S*)-lysyl hydroxylase

To date, characterized 2OG oxygenases catalyze hydroxylation at the C4 (e.g. JMJD414) and C5 (e.g. JMJD6 and the procollagen lysyl hydroxylases (PLODs)10,26) positions of lysyl side-chains. To investigate the regio- and stereo-selectivity of JMJD7, a DRG1 peptide was hydroxylated, then hydrolyzed and subjected to amino acid analysis. Following derivatization, LC-MS revealed a new peak, not present in controls, with a mass corresponding to derivatized hydroxylysine (obsvd. 503.2162 Da; calcd. 503.2037 Da). Comparison using C3-, C4-, and C5- hydroxylysine standards14 reveals the product co-elutes with one of the C3 hydroxylysine enantiomeric pairs (Fig. 4a and Supplementary Fig.

19); C3 hydroxylation is supported by NMR analyses of hydroxylated DRG1 and DRG2 peptides (Supplementary Fig. 20). Comparison with a diastereomeric mixture of C3 hydroxylysine isomers and synthetic (2*S*,3*R*)/(2*R*,3*S*)-hydroxylysine standard27 identified (2*S*,*3S*)-hydroxylysine as the JMJD7-catalyzed product (Fig. 4b and Supplementary Fig. 19c-d). No evidence for other isomers was observed within detection limits, revealing JMJD7 stereospecifically catalyzes (3*S*)-hydroxylation (Fig. 4a-c; assuming retention of (*2S*)-stereochemistry), a previously undescribed PTM.

DRG hydroxylation promotes ribonucleic acid binding

The effect of C3 lysyl hydroxylation on *in vitro* proteolysis suggests that this novel PTM can regulate intramolecular interactions with functional consequences. We therefore explored potential biological roles of DRG C3 lysyl hydroxylation. Unlike HIF hydroxylases, JMJD7 did not significantly regulate substrate levels: Overexpression of wildtype or H178A JMJD7 (Fig. 2a and Supplementary Fig. 9b-d), treatment with DMOG (Supplementary Fig. 9b-d), or DRG hydroxylation site mutation (Supplementary Figs 21 and 22) did not consistently affect the expression of DRG or DFRP proteins in cells. Furthermore, hydroxylation did not, within detection limits, change the thermal stability of full-length, isolated DRG1 (using differential scanning calorimetry; Supplementary Fig. 23). Consistent with a lack of effect on cellular stability, hydroxylation site substituted DRGs did not affect their ability to co-precipitate DFRPs, which are major regulators of DRG protein turnover22 (Supplementary Fig. 21). Hydroxylation also did not consistently affect GTPase activity, as determined by ^{1}H NMR or phosphate release assays using recombinant DRG1 *in vitro* (Supplementary Fig. 24), or using DRG1/2 purified from cells exposed to JMJD7 overexpression, shRNA knockdown, or DMOG treatment (Supplementary Fig. 25).

As described above, the lysine residue targeted by JMJD7 is located at the apex of a highly conserved HTH motif within the *N*-terminal regions of DRG1/2 (Supplementary Fig. 15c). Although the role of this domain has not previously been reported, yeast complementation studies reveal it is critical for DRG function28. JMJD7-mediated DRG hydroxylation is analogous to JMJD4-mediated eRF1 hydroxylation (Supplementary Fig. 15c-d), in the sense that both are lysyl hydroxylation events targeting HTH domains. eRF1 lysyl hydroxylation is thought to promote translation termination by supporting the interaction of eRF1 with the mRNA stop codon14, raising the possibility that DRG lysyl hydroxylation catalyzed by JMJD7 has a related function. Indeed, we observed significant binding of DRG2 to RNA affinity columns (Supplementary Fig. 22; consistent with previous reports29). Furthermore, a DRG2 K21 mutant had reduced affinity, thus localizing RNA binding activity to the HTH domain (Supplementary Fig. 22). Importantly, shRNA-mediated JMJD7 knockdown also reduced the RNA binding affinity of purified DRG2 (Fig. 4d and Supplementary Fig. 22d). These data support a role for JMJD7-mediated C3 lysyl hydroxylation in promoting the interaction of the DRG TRAFAC GTPases with RNA. Future work can focus on defining the precise nature of the JMJD7-DRG-DFRP ribonucleoprotein complexes and their biological roles.

Europe PMC Funders Author Manuscripts

Discussion

The combined cellular and biochemical results demonstrate that JMJD7 targets highly conserved lysine residues within 2 closely related TRAFAC GTPase proteins. The finding that JMJD7 catalyzes *(3S)*-lysyl hydroxylation, the first time this PTM has been observed in humans, expands the repertoire of 2OG oxygenase-catalyzed modifications of basic residues, which also include histidinyl-hydroxylation12,30, lysyl C4 hydroxylation14, lysyl (5*S*)- and (5*R*)-hydroxylation24,26, N^{ε}-methyl lysyl demethylation31, argininyl C3 hydroxylation12 and, possibly, N-methyl argininyl-demethylation32. The extent of 2OG oxygenase-catalyzed lysyl hydroxylation is striking. With the discovery of JMJD7-catalyzed C3 lysyl hydroxylation, a total of seven different lysine residues oxidations are now known to be catalyzed by 2OG oxygenases. Aside from the 'not (yet) observed' C3 and C4 stereoisomers, oxidation at the C2 and C6 positions are unidentified exceptions; although the products of such reactions are likely unstable, they have precedent in 2OG oxygenase catalyzed protein fragmentation (albeit not at lysine residues as yet) via C2 hydroxylation33.

In most cases, the detailed biochemical roles of lysyl hydroxylations are unclear, with the enablement of glycosylation by procollagen (5*R*)-lysyl hydroxylation26 and improved stop codon decoding by C4 lysyl hydroxylation14,34,35 being exceptions. Our experiments indicate that JMJD7-catalyzed hydroxylation does not substantially effect on the intrinsic stability, protein expression, or GTPase activity of DRGs. Interestingly, however, we observed that JMJD7-catalyzed C3 lysyl hydroxylation clearly impairs experimental proteolysis, at either the *C*- or *N*-terminal sides of the target lysyl-residue. While inhibition of the tested proteases is likely not biologically relevant, this observation raises the possibility of a wider role for protein hydroxylation in directly modulating protease hydrolysis. This is particularly attractive for C3 lysyl-hydroxylation and nucleophilic serine/threonine protease inhibition, where work with proteases and bacterial cell wall biosynthesis enzymes employing nucleophilic serine catalysis has revealed that substrate/inhibitor substitutions that perturb hydrolysis (or formation) of the acyl-enzyme complex can lead to inhibition36.

In addition to effects on protease hydrolysis, we observed JMJD7- and hydroxylation site-dependent regulation of RNA binding, analogous to the role of JMJD4 in promoting mRNA stop codon decoding by eRF114. Although future work is required to address the physiological RNA targets, the presence of DRGs in ribosome fractions from diverse species including yeasts, plants, and humans28,37,38 could be consistent with an interaction with messenger or ribosomal RNA. Although the biochemical role of the DRGs in protein translation is unclear, it is consistent with their similarity to other OBG GTPases of the TRAFAC family, which have roles in ribosome biogenesis and translation control23,39. A prokaryotic 2OG-dependent prolyl hydroxylase homologous with the animal HIF prolyl hydroxylases, Elongation Factor Thermo unstable (EF-Tu), has also been found to catalyze hydroxylation of a loop region of a translation-associated GTPase40; thus, physical and functional interactions between 2OG oxygenases, translation factors, and RNA may have ancient origins.

The discovery of JMJD7-catalyzed DRG hydroxylation contributes to growing evidence on the importance of the dynamic interactions between 2OG oxygenases and their substrates/interacting partners in disease6,41. Both JMJD7 and DRG1/DRG2 are linked to cell growth in diverse cell types and species29,37,42–44. JMJD7 and DRG1/2 may also have context dependent roles in diseases including cancer and mental disorders; the *DRG2* gene is located in a chromosomal region implicated in the Smith-Magenis neurobehavioral syndrome45, and DRG1/2 SNPs have been identified in a screen of candidate genes for autism spectrum disorders46. In support of this, genetic studies in high-risk autism families and persons with severe intellectual disabilities have identified 2 substitutions in the *JMJD7* gene20,47. Future work can now address whether JMJD7-catalyzed hydroxylation of DRG1/2 regulates protein synthesis and how this underlies the role of this novel pathway in growth control and disease.

Online Methods

Analysis of growth phenotypes in *Drosophila melanogaster*

Drosophila maintenance, engineering, and knockdowns were performed as described48. Flies used in this study were en-Gal4 from the Bloominton *Drosophila* stock center and white RNAi (as a control) and *CG10133* RNAi from the VDRC stock center. For analysis of growth phenotypes, wings from 4 day old females and males were removed and mounted in a solution containing 1:1 lactic acid/ethanol. Wings were imaged using an Olympus MVX10 stereomicroscope connected to an Olympus DP71 digital camera, and variations in the area of the posterior compartment were estimated by measuring the area comprised between veins L4, PCV and L5, using the ImageJ software (NIH, USA). To quantify variations of cell size, the number of wing hairs per square mm was counted from images taken with an Olympus BX60 microscope connected to an Olympus DP71 digital camera.

Mammalian cell culture and transfection

Human tumor and HEK293T cell lines were cultured in DMEM supplemented with 10% FBS (Sigma) and 1% penicillin-streptomycin at 37°C in a humidified atmosphere with 5% CO_2. Plasmids were transfected using FuGENE6 Transfection Reagent (Promega) according to manufacturer's instructions. siRNA oligonucleotides (Sigma MISSION) were transfected twice over consecutive days at a concentration of 25 nM using OligoFectamine (ThermoFisher), according to the manufacturer's instructions. Lentiviral particles containing doxycyline-inducible cDNA expression and shRNA vectors were generated by co-transfection of HEK293T cells with 2nd generation vectors (pMD2.G and psPAX2) and used to create puromycin-resistant stable lines in HeLa, HEK293T, A549 and SW620 cells. Doxycycline-inducible control and JMJD7 shRNA lentiviral vectors were from the pZIP-TRE3G shERWOOD Ultramir collection and purchased from Transomic.

Statistics, Reagents, and Animal Models

Validated antibodies used in this study included those raised against HA-tag (BioLegend, clone 16B12), DRG1 (Proteintech, 13190-1-AP), DRG2 (Proteintech, 14743-1-AP), JMJD7 (St Johns Laboratory, STJ29545), JMJD4 (Ximbio, 152745), DFRP1 (SIGMA, HPA031099), DFRP2 (GeneTex, GTX120331), β-actin (Abcam, ab8227), FLAG (SIGMA,

A8592), and V5 (BioRad, MCA1360P). HEK293T, HeLa, U2OS, A549, and SW620 cell lines were purchased from the ATCC and tested for mycoplasma contamination every 3 months. Cells lined are further validated by STR profiling as part of a rolling program. Statistical analyses generally involved calculation of mean and standard deviation or standard error of data obtained from a minimum of three biologically independent samples. Assays with recombinant proteins were carried out (at least) in technical triplicate. Sample sizes were designed based on prior assay experience, similar work on related projects, and pilot data.

Expression vectors and site-directed mutagenesis

JMJD7, *DRG1*, *DRG2*, *DFRP1*, *DFRP2* and *dmJMJD7* cDNA were cloned into the pCDNA3 vector (ThermoFisher) by PCR to incorporate the indicated *N*-terminal epitope tags. JMJD7 and variants with *N*-terminal 3x-FLAG tags were cloned into the RFP site of the doxycycline-inducible pTRIPZ vector (GE LifeSciences) ('pTIPZ'). The pET28a-JMJD7 plasmid was prepared by Dr. Wei Ge and generated by inserting the human *JMJD7* gene (encoding full-length JMJD7, residues 1-316, NCBI gene accession number: 100137047) into the pET28a vector (Novagen) for production in *Escherichia coli* with an *N*-terminal His_6-tag and a thrombin protease cleavage site (MGSSHHHHHHSSGLVPR*GSH). The following human JMJD7 constructs (residues 1-316, 1-295, 27-316, 27-295), which were used to investigate oligomerization of JMJD7, were amplified from pET28a-JMJD7 using custom primers (Sigma Aldrich) and cloned into the pNIC28-Bsa4 vector using ligation-independent cloning, resulting in constructs with an *N*-terminal His_6-tag and tobacco etch virus (TEV) protease cleavage site (MHHHHHHSSGVDLGTENLYFQ*SM). Genes encoding for full-length DRG1 (residues 1-367, NCBI gene accession number: 4733) and DRG2 (residues 1-364; NCBI gene accession number: 1819) were amplified from U2-OS cDNA (kindly provided by Dr Louise Walport, University of Oxford) and also inserted into the pNIC28-Bsa4 vector. Site-directed mutagenesis was performed using custom primers (Invitrogen or Sigma Aldrich) and either Phusion High-Fidelity PCR Master Mix with HF Buffer (NEB) or the Stratagene QuikChange® method with Q5 High-Fidelity DNA Polymerase (NEB). PCR was carried out according to the manufacturer's recommendations followed by DpnI (Thermo-Fisher) digestion for 60 minutes at 37°C before DNA purification and bacterial transformation. All constructs were fully DNA sequence verified.

Immunofluorescence

HeLa cells were seeded onto glass cover slips the day before transfection with pCDNA3 FLAG-JMJD7 and/or HA-DRG1/2. After 48 hours, cells were washed three times with cold PBS before fixing and permeabilizing with 100% acetone for 7 minutes at -20°C. Immunofluorescence co-staining was achieved by incubating samples with primary antibodies at 4°C overnight. Secondary antibodies (Alexa Fluor 555 anti-mouse and Alexa Fluor 488nm anti-rabbit (ThermoFisher)) were incubated at 1:2,000 for 1 hour at room temperature prior to DAPI (Sigma) staining. Cover slips were mounted onto slides using anti-fade mounting media (NEB ProLong Gold) and imaged using Zeiss LSM510.

Protein expression analyses

Cellular proteins were extracted using either JIES (20 mM Tris·HCl pH 7.4, 100 mM NaCl, 5 mM $MgCl_2$, 0.5% (v/v) Igepal CA-630, and Complete protease inhibitors (Roche)) or RIPA buffer. Protein extracts were quantified and equalized using Pierce 660nm Protein Assay Reagent. Western blotting antibodies were as described above. Signals were developed using SuperSignal West Pico, Dura, or Femto chemiluminescent substrates (Thermo Fisher Scientific).

JMJD7 proteomic screen

Inducible FLAG-JMJD7 stable cell lines (wildtype and H178A variant) were treated with doxycycline (SIGMA) for 38 hours before the addition of 1 mM dimethyl-*N*-oxalylglycine (DMOG; SIGMA, D3695) for 16 hours, to trap substrates. Cells were lysed in JIES in the presence of 1 mM *N*-oxalylglycine (NOG; Cambridge Bioscience, 13944), prior to immunoprecipitation with anti-FLAG M2 Magnetic Beads (Sigma, M8823), overnight at 4°C with rotation. Samples were then washed six times in JIES before elution with 100 μg/ml 3x-FLAG peptide (SIGMA, F4799). Eluents were desalted by methanol:chloroform extraction prior to in-solution trypsin digestion using standard methods49. Purified tryptic peptides were analyzed by mass spectrometry (as detailed below) in technical triplicates to allow for label-free quantification.

JMJD7:DRG interaction assays

Doxycycline-inducible FLAG-JMJD7 stable cell lines were treated with doxycycline as above before the addition, or not, of 1 mM DMOG for 10-16 hours. Cells were lysed in JIES in the presence or absence of 1 mM NOG prior to immunoprecipitation with anti-FLAG Beads, overnight at 4°C with rotation. Samples were then washed six times in JIES before elution with 100 μg/ml 3x-FLAG peptide. The interaction of transfected FLAG-DRG1/2 with endogenous JMJD7 was explored using an identical approach. Endogenous DRG/DFRP/JMJD7 complexes were analyzed by immunoprecipitation from large-scale DMOG-treated HEK293T cell extracts using DFRP antibodies bound to protein A agarose (Millipore) and eluted with 2x Laemmli buffer.

DRG purification for MS analyses

For exogenous DRG analyses, HEK293T cells were transfected with the pCDNA3 HA-DRG1/V5-DFRP1 or pCDNA3 HA-DRG2/V5-DFRP2 vectors in the presence or absence of pCDNA3 FLAG-JMJD7. Cells were incubated under standard culture conditions for 48 hours before lysis in JIES buffer and immunoaffinity purification of DRG/DFRP complexes using anti-HA agarose beads (SIGMA, A2095) at 4°C for 16 hours with rotation. Beads were washed five times with JIES before elution with anti-HA peptide (SIGMA, I2149), protease digest, and mass spectrometry analysis. For endogenous DRG analyses, large-scale cell cultures were lysed in JIES buffer before immunoaffinity purification using the antibodies described above. Beads were washed with JIES buffer and eluted with 2X Laemmli buffer and separated by SDS-PAGE. DRG1 and DRG2 protein bands were excised from Coomassie-stained gels prior to protease digest and mass spectrometry analysis.

Europe PMC Funders Author Manuscripts

RNA interaction assays

HEK293T cells were transfected with pcDNA3 FLAG-DRG1, -DRG1-K22A, -DRG2 or DRG2-K21A. Alternatively, stable HEK293T cell lines expressing conditional control and JMJD7 shRNA were treated with 1 μg/ml doxycycline for 72h prior to transfection with pCDNA3 FLAG-DRG2. Forty-eight hours after transfections cells were lysed in JIES buffer, then centrifuged (14,000 rpm, 10 minutes) to remove cell debris. Protein extracts were used directly in RNA pulldown assays, or were subject to anti-FLAG immunoprecipitation and elution (as above) to purify FLAG-DRG proteins for use in RNA pulldown assays (in the presence of JIES buffer supplemented with 1mM DTT). Samples were incubated with either 4 mg polycytidylic acid-Agarose beads (SIGMA, P9827), 4 mg polyuridylic acid-Agarose beads (SIGMA, P8563) or 20 μl control Protein A Agarose beads (Millipore, 16-156) at 4°C for 2 hours with rotation. Beads were washed five times with JIES before elution with 30 μl 2X Laemmli buffer.

Cellular Protein Mass Spectrometry

Protein samples were digested and desalted using standard methods for in-gel50 and in-solution49 digest. Desalted samples were analyzed by nLC-MS/MS with frontend separation using a Dionex Ultimate 3000 UPLC at a flowrate of 250 nl/min. Peptides were separated using a PepMAP C18 column (75 μm × 500 mm, 2 μm particle size) and a one hour gradient of 2-35% Acetonitrile in 5% DMSO/0.1% formic acid. For MS detection, we either used a Q-Exactive, Q-Exactive HF or Orbitrap Fusion Lumos (all Thermo) in HCD mode (Q-Exactives) or CID/Ion trap detection mode for MS/MS data acquisition with the following parameters:

	Q-Exactive	Q-Exactive HF	Orbitrap Fusion Lumos
Resolution MS1	70000	60000	120000
Resolution MS2/Scan rate	17500	30000	rapid
MS1 scan range	380 to 1800 m/z	375 to 1500 m/z	375 to 1500 m/z
MS2 scan range	200 to 2000 m/z	200 to 2000	auto
pAGC target MS1	3.00E+06	3.00E+06	4.00E+05
pAGC target MS2	1.00E+05	5.00E+04	2.00E+03
Top N/Speed	15	12	3 s
Dynamic Exclusion	27 s	27 s	60 s
max. injection time MS1	100 ms	45 ms	50
max. injection time MS2	128 ms	100 ms	250
Normalized collision energy	28	28	35
Activation	HCD	HCD	CID
MS2 detector	Orbitrap	Orbitrap	Linear Ion Trap

Data were searched against the UniProt Reference (UPR) *Homo sapiens* database (retrieved 15.10.2014) with PEAKS Studio 7.5 (Bioinformatics Solutions) with 10 ppm mass error tolerance for precursor mass and 0.05 Da (Q-Exactives) / 0.5 Da (Orbitrap Fusion Lumos)

tolerance for fragment masses. Carbamidomethylation on cysteine was selected as a 'fixed' modification, while oxidation (M), deamidation (N, Q) and hydroxylation (P, K, D, N, R, Y) were selected as variable modifications for the database search. Using a target/decoy fusion approach, the peptide false discovery rate was set to 1%. Peptide abundance was measured as accumulated ion counts after extraction of the chromatographic elution profile of the precursor mass of interest using Qual Browser, Xcalibur 3.0.63 (Thermo).

In vitro JMJD7:DRG interaction assay

HA-DRG1, -DRG1-K22A, -DRG2, and -DRG2-K21A proteins were produced *in vitro* using the TNT Quick-Coupled transcription/translation system (Promega, L1170). IVVT reactions and anti-FLAG M2 Magnetic Beads (Sigma, m8823) were spiked into HEK293T cell lysates expressing either pCDNA3 or pCDNA3-FLAG-JMJD7 prior to overnight incubation at 4°C for 16 hours with rotation. Anti-FLAG beads were washed three times with JIES buffer before eluting with 50 µl 2X Laemmli buffer.

Protein Basic Local Alignment Search Tool (BLAST) DRG1/2 analysis

Protein BLAST® (https://blast.ncbi.nlm.nih.gov/Blast.cgi?PAGE=Proteins) searches identified DRG1/2 homologs from indicated organisms using the human protein sequence as the entry query (NCBI Reference IDs – *H. sapiens:* NP_004138.1/001379.1; *X. laevis:* 001084013.1/001079983.1; *D. melanogaster:* 536733.1/650822.1; *C. elegans:* 001255126.1/498808.2; *A. thaliana:* 195662.1/173190.1; *S. cerevisiae:* 009364.1/011689.1; *D. discoideum:* 636294.1/641633.1; *T. thermophila:* 001025967.2/001021328.1). Sequences were aligned using Clustal Omega (https://www.ebi.ac.uk/Tools/msa/clustalo/) and shaded using GeneDoc (version 2.7) as shown in Fig. 3A.

Recombinant protein production and purification

All recombinant JMJD7 proteins were produced with *N*-terminal His_6-tags in *E. coli* Rosetta™ (DE3)pLysS cells (Novagen). Cells were grown in 2TY media at 37°C to an OD_{600} of 0.6-0.8. Recombinant protein production was induced with 0.5 mM isopropyl β-D-1-thiogalactopyrandoside (ITPG); cells were then grown overnight at 18°C. Proteins were purified by nickel affinity chromatography using an AKTA FPLC system (GE Healthcare®). Recombinant protein was eluted from the column using a stepwise gradient (30 – 250 mM imidazole), and protein-containing fractions were further purified by size exclusion chromatography using a Superdex 75 10/300 GL column (Amersham Pharmacia Biosciences). Protein purity was assessed by SDS-PAGE analysis and subsequently pooled, concentrated (10-25 mg/mL), flash frozen in liquid nitrogen, then stored at -80°C in 50 mM Hepes, 200 mM NaCl, 2% glycerol, pH 7.5.

Recombinant DRG1 was produced and purified as reported51. The TEV protease was used for His_6-tag cleavage (1:20, TEV:DRG1) with overnight treatment at 4 °C. DRG1 was collected as the eluent after a 5 mL HiTrap nickel column treatment. DRG1 purity was validated by SDS-PAGE and MS analyses.

Recombinant DRG1 hydroxylation

Purified, full-length DRG1 was hydroxylated by treatment with His_6-JMJD7. Assay mixtures contained 50 μM DRG1, 2 μM JMJD7, 100 μM ammonium iron(II) sulphate hexahydrate (Fe(II)), 500 μM 2-oxoglutarate acid disodium salt (2OG), 1 mM (+)-sodium L-ascorbate (ascorbate) in 50 mM HEPES, 500 mM NaCl, 5% glycerol, pH 7.5. The reaction was carried out for 2 h at 37°C. Hydroxylated DRG1 was collected as the eluent after a 5 mL HiTrap nickel column treatment. Hydroxylation was confirmed by MS analysis using a Xevo GS-2-S mass spectrometer (Waters). >95% hydroxylation, as observed by MS, was achieved under the stated conditions. The concentration of the hydroxylated samples was determined using a ND-1000 Spectrophotometer (Nanodrop Technologies).

Peptide synthesis

The 25-mer $DRG1_{16-40}$ (ARTQKNKATAHHLGLLKARLAKLRR-NH_2, >95%) and $DRG2_{15-39}$ (ARTQKNKATEYHLGLLKAKLAKYRA-NH_2, >95%) peptides) were commercially synthesized with *C*-terminal amides by either Severn Biotech (United Kingdom) or GL BioChem (China).

The $DRG1_{21-40}$ peptide (NKATAHHLGLLKARLAKLRR-NH_2) was synthesized in house by solid phase synthesis using a Liberty Blue automated microwave peptide synthesizer (CEM Corporation, USA) for amino acid analysis as described32. All other peptides used for screening were synthesized using a Multipep RSi solid phase peptide synthesizer (Intavis AG Bioanalytical Instruments, Germany) on a plate module (1-5 mg scale) using Tentagel S-RAM resin as described32. All peptides were synthesized as *C*-terminal amides. The $DRG1_{21-40}$ peptide used for amino acid analysis was purified by reverse-phase high-performance liquid chromatography using a Vydac C18 column (Solvent A = 0.1% trifluoroacetic acid in water; Solvent B = 0.1% trifluoroacetic acid in acetonitrile) to >90% purity as determined by LC-MS. Peptides used for screening assays were not purified.

JMJD7 activity assays

JMJD7 NMR activity assays—NMR assays were carried out as described32. 160 μL reactions were prepared in a 1.5 mL Eppendorf tube with 16 μL D_2O (Sigma-Aldrich), ±100 μM Fe(II), 200 μM 2OG, ±500 μM ascorbate, ±1 mM NOG, ±10 μM JMJD7, and ±10 μM JMJD7-H178A in 20 mM Tris D-11 (Cambridge Isotope Laboratories), pH 7.5. Reactions were initiated by addition of JMJD7 or JMJD7-H178A and immediately transferred to a 3 mm Shigemi NMR tube, which was centrifuged for a few seconds in a hand centrifuge. Proton NMR spectra were acquired, and the reaction was monitored in real-time on a Bruker Avance III 700 MHz spectrometer equipped with a 5 mm inverse TCI cryoprobe at 298K and controlled by TopSpin 3.5. The AV700 was controlled by TopSpin software, and spectrometer conditions were optimized using a control sample with all reaction components except JMJD7 prior to data acquisition. The first proton spectrum was acquired with water suppression (16 scans), 325 s after mixing, following brief optimization (start of data acquisition was 225 s). Spectra were automatically acquired every 105 s for 1900 s. TopSpin 3.2 software was used to process and integrate the peaks corresponding to 2OG and succinate for analysis using Microsoft Excel 2003.

MALDI-MS hydroxylation assays—JMJD7 assay mixtures (final volume 20 μL in 50 mM HEPES, pH 7.5) containing 50 μM peptide and 10 μM His_6-JMJD7 were incubated for 60 minutes at 37°C with 100 μM Fe(II), 200 μM 2OG, and 500 ascorbate. Reactions were quenched by immediately spotting 1 μL of assay sample and 1 μL of α-cyano-4-hydroxycinnamic acid (CHCA) matrix solution (saturated CHCA in 50% acetonitrile, 50% water, 0.1% trifluoroacetic acid) onto a Waters 96-spot MALDI plate. The samples were analyzed using MALDI- MS and a Waters Micromass™ MALDI micro MX™ instrument in the positive ion reflectron mode. MALDI-MS spectra were analyzed using MassLynx 4.1 (Waters) by baseline subtraction (polynomial order, 15; below curve %, 10; tolerance, 0.01) and smoothing (number of smooths, 2; smooth window channels, 10; Savitzky-Golay).

Co-factor/substrate dependence assays—Co-factor/substrate dependence assays (Fig. 3d) were performed as described (above) with the following modifications: 50 μM $DRG1_{16\text{-}40}$, ±1 μM JMJD7 or JMJD7-H178A, ±100 μM Fe(II), ±500 μM 2OG, ± 1mM ascorbate, ± 1mM NOG, and quenching after 5 minutes of incubation at 37°C with formic acid (2% final concentration) prior to spotting on the MALDI plate.

$^{18}O_2$ incorporation assays—Hydroxylation of $DRG1_{16\text{-}40}$ by JMJD7 was performed under atmospheres of argon, $^{16}O_2$, or $^{18}O_2$ (CK Isotopes, 98%) as described12. Assays were performed under the following conditions: 50 μM $DRG1_{16\text{-}40}$, ±2.5 μM JMJD7, 100 μM Fe(II), 500 μM 2OG, and 1 mM ascorbate in 50 mM HEPES, pH 7.5. A solution of peptide and buffer (94 μL) in a septum-sealed glass vial was purged with N_2 for 30 minutes on ice using a mass flow controller (Brooks Instruments) and an escape needle. 1μL of 2OG, Fe(II), ascorbate, and JMJD7 were then sequentially added on ice using gastight Hamiltonian syringes. A balloon attached to a syringe was purged 3x with Argon then filled with the gas of choice (argon, $^{16}O_2$, and $^{18}O_2$). The reaction was initiated by slowly bubbling the gas into the solution at room temperature using an escape needle until the balloon was deflated (~10 minutes). The escape needle was removed, followed by the balloon; the solution was then incubated at 37°C for an additional 20 minutes and quenched with 100 μL of 4% formic acid. Products were analyzed by MALDI-MS as above.

Non-denaturing MS

Stoichiometry measurements were performed using a hybrid quadrupole-Orbitrap (Thermo QExactive) and a quadrupole-time-of-flight (Waters Synapt G2Si) instrument for detection of high mass ions52,53. Samples (10 μM) were buffer exchanged into 200 mM ammonium acetate using Bio-spin 6 (Bio-Rad) centrifuge columns immediately prior to analysis. Ions were generated by static nanoelectrospray using gold-coated capillaries prepared in-house. Data were obtained with a wide acquisition window (2,000-10,000 *m/z*); desolvation was achieved with moderate HCD voltage (QExactive; 10-50 V) or CID (Synapt; 4 V) applied. Instrument settings were: (QExactive): capillary voltage = 1.1 kV; source temperature = 50°C; max injection time = 50; S-lens RF = 100; C-trap entrance lens = 5.8. Spectra were obtained with 10 microscans, averaged over 100 scans. Instrument settings were as follows (Synapt): capillary voltage = 1.4 kV; source temperature = 50°C; sample cone = 10 V; trap DC bias = 10 V. Data were processed using XCalibur 2.1 (Thermo Scientific) and MassLynx

Europe PMC Funders Author Manuscripts

V4.1 (Waters) software and masses were assigned using in-house software (Mass/Charge State Error Determination v 0.3; http://benesch.chem.ox.ac.uk/resources.html).

SEC-MALS and CD studies

Analysis of JMJD7 was performed using an Agilent 1260 HPLC with a Superdex 200 Increase 3.2/300 SEC column (GE Healthcare) coupled to a DAWN HELEOS II scattering detector (Wyatt Technologies) and Optilab T-rEX (Wyatt Technologies) differential refractive index detector. The MALS detector was equilibrated overnight in running buffer to ensure minimal background light scattering. ~30 μg of protein was loaded on-column (column compartment was set to 20°C) at a flow rate of 75 μL/min in 50 mM HEPES, 200 mM NaCl, 2% glycerol, pH 7.5. Data acquisition and analysis were performed with Astra 6.1 software (Wyatt Technologies).

CD spectra were acquired using a Chirascan CD spectrometer (Applied Photophysics model) equipped with a Peltier temperature-control cell holder. Experiments were performed at 20°C in a 0.1 cm pathlength cuvette using 0.2 mg/mL of protein in 10 mM sodium phosphate buffer, pH 8.0. Data were recorded in triplicate from 260 to 185 nm in 0.5 nm steps with a 1 nm bandwidth. Spectral data were baseline corrected, averaged, and smoothed using the Savitzky-Golay filter (smooth = 8).

Peptide NMR analyses

$DRG1_{16-40}$ and $DRG2_{15-39}$ peptides (~1.4 mg) were incubated with 2 μM JMJD7, 100 μM Fe(II), 500 μM 2OG, 1 mM ascorbate in 50 mM HEPES, pH 7.5 (10 mL reaction volume) for 2 hours at 37°C; reactions were quenched by adding neat formic acid dropwise until pH ~2. Peptides were purified using two Sep Pak C18 columns in tandem according to the Kessler Laboratory Proteomics Protocol (University of Oxford, http://www.ccmp.ox.ac.uk/_asset/file/sep-pak-c18.pdf; all volumes doubled), eluting with 4 mL of 40% acetonitrile, 0.1% formic acid solution in double distilled water. Samples were then dried by vacuum centrifugation and resuspended in H_2O/D_2O (9:1) for 2D NMR analyses (HSQC, HMBC, COSY, TOCSY). Spectra were recorded using a Bruker AVIII 700 MHz NMR spectrometer equipped with a 5-mm inverse cryoprobe using 3mm MATCH NMR tubes (Cortecnet). Data were processed using a TopSpin 3.2 software (Bruker).

Amino acid analyses

Sample Preparation—Peptides (50 μM; $DRG1_{21-40}$, $DRG1_{16-40}$, and $DRG2_{15-39}$) were incubated with 100 μM Fe(II), 200 μM 2OG, and 500 μM ascorbate in the presence or absence of 10 μM recombinant His_6-JMJD7 for 1 hour at 37°C in 50 mM HEPES, pH 7.5 (final volume 500 μL). The reaction was quenched with 2 drops of neat formic acid; hydroxylation (~40-80%) of the peptide was confirmed by MALDI-MS. Recombinant JMJD7 was removed using a Sep Pak C18 column according to the Kessler Lab Proteomics Protocol (University of Oxford, http://www.ccmp.ox.ac.uk/_asset/file/sep-pak-c18.pdf), eluting with a 15% acetonitrile, 0.1% formic acid solution in double distilled water. Samples were then dried by vacuum centrifugation and subsequently re-suspended in 60 μL of 20 mM HEPES, pH 7.5. Enzymatic hydrolysis was carried out at 37°C with a non-specific protease from *Streptomyces griseus* (9 μL, 1 mg mL^{-1}, Sigma-Aldrich) overnight.

LC-MS analyses—Hydrolyzed samples were dried by vacuum centrifugation followed by resuspension in borate buffer and derivatization with 6-aminoquinolyl-*N*-hydroxysuccinimidyl carbamate (AQC) according to the AccQ-Tag Ultra Derivatization Protocol (Waters). LC-MS analyses were performed as described 24, using a Waters Acquity ultra performance liquid chromatography system coupled to a Xevo G2-S QTof mass spectrometer equipped with an electrospray ionisation source. Gradient conditions for separation were carried out as described in either the AccQ-Tag Ultra Derivatization Protocol (Waters; 10 minute gradient) or in Feng et al., 201414 (30 minute gradient).

Conditions for ESI-MS detection: mode, positive-ion; analyzer, resolution mode; desolvation temperature, 600°C; source temperature,100°C, capillary voltage, 3000 V; sample cone voltage, 20 V; cone gas flow, 30 L/min; and desolvation gas flow 1000 L/min. MS data were acquired and extracted ion chromatograms were produced for m/z values of either 503.2, corresponding to the theoretical masses of AQC-derivatized hydroxylysine (503.2037). Extracted ion chromatograms were smoothed (number of smooths, 2; smooth window channels, 3; Savitzky-Golay) and total ion current chromatograms were further baseline subtracted (polynomial order, 1; below curve %, 40; tolerance, 0.01).

C3, C4, and C5 hydroxylysine standards were synthesized or commercially obtained as described14. The synthesis of the (2*S*,3*R*)/(2*R*,2*S*)-3-hydroxylysine standard has been reported elsewhere27.

Differential scanning calorimtery

Differential scanning calorimetry experiments were performed on a Malvern (Malvern, UK) VP Capillary DSC instrument at the Department of Biochemistry, University of Oxford. Samples and buffer blanks were measured using a thermal ramp of 200 °C/hr between 10°C and 110°C at a pressure of 55 psi. Samples contained 80 μM full length DRG1/hydroxylated DRG1 in the presence or absence of 1 mM GDP (Sigma) in 50 mM HEPES, 500 mM NaCl, 5 % glycerol, pH 7.5. The buffer blanks consisted of 50 mM HEPES, 500 mM NaCl, 5 % glycerol, pH 7.5 (± 1 mM GDP).

DRG GTPase activity assays

Phosphate release assay—GTP hydrolysis was measured using a colorimetric assay for determination of phosphate release51. Recombinant, full length DRG1 and hydroxylated DRG1 (10 μM) were incubated with increasing concentrations (0–4 mM) of GTP in 100 mM Tris/HCl, pH 8, 300 mM KCl, 20 mM $MgCl_2$, 10% glycerol at 37 °C for 60 min. Reactions were stopped by adding 50 μL of fresh malachite green reagent. This reagent contained 2 volumes of 0.0812% malachite green, 2 volumes of bidistilled water, 1 volume of ammonium molybdate (5.72% in 6 M HCl) and 1 volume of 2.32% polyvinyl alcohol (Phosphate Assay Kit, colorimetric, Abcam). The samples were read within the next 10 min in a PheraStar plate reader at 650 nm using half-area, medium binding, clear bottom plates (Fischer Scientific). End-point assays contained the purified proteins (10 μM) that were incubated with 1 mM of GTP in 100 mM Tris/HCl, pH 8, 300 mM KCl, 20 mM $MgCl_2$, 10% glycerol at 42°C for 60 min. The samples were quenched and read as previously stated.

GTPase activity monitoring by NMR—Purified proteins (40 μM) were incubated with 4 mM of GTP in 50 mM Tris-D_{11}, pH 7.5, 300 mM KCl, 20 mM $MgCl_2$, at 37 °C for 60 min. Controls contained 4 mM GTP or GDP under the same conditions. ^{1}H excitation sculpting suppression NMR spectra were recorded using a Bruker AVIII 600 MHz NMR spectrometer equipped with a BB-F/^{1}H Prodigy N_2 cryoprobe using 5 mm diameter NMR tubes (Norell). Spectra were typically obtained using 252 scans, a relaxation delay of 1 s, and a prescan delay of 10 μs. A 2 ms sinc pulse was used for water suppression. Data were processed with a line broadening of 0.3 Hz using TopSpin 3.2 software (Bruker).

GTPase activity assay of DRG proteins purified from human cells—FLAG-DRG1/2 proteins and mutants were expressed in HEK293T cells under a variety of conditions, including: co-expression of HA-JMJD7, knockdown of JMJD7 by shRNA (as detailed above), or DMOG treatment (1 mM for 16 hours). Cells were lysed in JIES prior to anti-FLAG immunoprecipitation. Beads were then washed six times in JIES before elution with 100 μg/ml 3x-FLAG peptide in 100 mm Tris-HCl pH 8, 200 mM KCl, 20 mM $MgCl_2$, 10% (v/v) glycerol. The purity and abundance of DRG1/2 proteins were determined by SDS-PAGE and coomassie staining. GTPase activity of purified proteins was measured using the GTPase-Glo Kit (Promega, V7681), according to the manufacturer's guidelines, but with the following modifications. Firstly, the GTPase assay buffer was supplemented with 200 mM KCl to support DRG GTPase activity51. Secondly, assays were performed at 37°C for either 2h (DRG2) or 8h (DRG1).

Crystallization conditions

Crystals of His_6-JMJD7.Mn(II).2OG and His_6-JMJD7-R260C.Mn(II).2OG were obtained in sitting drops at 25°C. For wildtype JMJD7, drops were formed in a 1:1 ratio of a 25 mg/mL His_6-JMJD7, 2 mM $MnCl_2$, 4 mM 2OG solution with a 1.5 M sodium nitrate, 0.1 M sodium acetate, pH 4.6 solution. For the R260C variant, drops were formed in a 1:1 ratio of a 26 mg/mL His_6-JMJD7-R260C, 2 mM $MnCl_2$, 4 mM 2OG solution with a 1.5 M sodium nitrate, 0.1 M sodium acetate, pH 4.6 solution containing additives (0.25% β-Nicotinamide adenine dinucleotide phosphate tetrasodium salt, 0.25% Adenosine 5'-triphosphate disodium salt hydrate, 0.25% N-Acetyl-D-galactosamine, 0.25% Gentamicin sulfate salt hydrate, 0.02 M HEPES sodium pH 6.8). Crystals were cryoprotected with 25% glycerol before flash freezing in liquid nitrogen.

Data collection, structure solution, and refinement

Data were collected using single crystals at 100 K at the Diamond Light Source (DLS) beam lines I04 (PDB: 5NFN, λ=0.9795 Å) and I03 (PDB: 5NFO, λ=0.9795 Å) and processed using HKL200054.

His_6-JMJD7.Mn(II).2OG data were strongly anisotropic (the spread in values of the three principal components of scale factors is 62.37 $Å^2$), with resolution limits of 3.5 Å, 3.5 Å, and 3.0 Å along the reciprocal axes a*, b* and c* (at an F/σ cutoff of 3). The data were ellipsoidally truncated and anisotropically scaled using the 'STARANISO anisotropy & Bayesian estimation server' (http://staraniso.globalphasing.org/cgi-bin/staraniso.cgi) with intensities renormalized for structure solution and initial rounds of refinements. An

ensemble of models was generated by the ENSEMBLER built in PHENIX55 using crystal structures of the related JmjC-enzymes, FIH (PDB ID: 1H2K), TYW5 (PDB ID: 3AL5), JMJD5 (PDB ID: 4GJZ), and JMJD6 (PDB ID: 3K2O) as templates. To ensure maximum degree of accuracy, only JMJD7 residues that are highly conserved in these four JmjC-hydroxylases were included in the homology models. The wildtype JMJD7 structure was then solved by molecular replacement using PHASER56. An initial model was generated by PHENIX AUTOBUILD55, which included 82% of JMJD7 residues making up the four molecules in the asymmetric unit. Iterative cycles of model building and refinement using Buster57 were performed until converging R_{factor}/R_{free} no longer decreased. Final rounds of intensity-based refinements were performed using CNS58 and PHENIX55. JMJD7-R260C structure was solved by molecular replacement using PHASER56 with 2 molecules per asymmetric unit using the JMJD7-wt structure as the initial model and refined by CNS58/PHENIX55 until R_{factor}/R_{free} converged with iterative cycles model building using COOT59. MOLPROBITY60 was used to monitor the geometric quality of the models between refinement cycles. Water molecules were added to peaks (> 1.5 σ $2F_oF_c$) in electron density maps that were within H-bond distance to protein with reasonable geometry to form H-bonds.

Supplementary Material

Refer to Web version on PubMed Central for supplementary material.

Acknowledgements

We thank the Biotechnology and Biological Sciences Research Council (BB/L009846/1, CJS), Medical Research Council (MR/N021053/1, MLC), Wellcome Trust (106244/Z/14/Z, CJS), Cancer Research UK (24552, MLC), University of Oxford Clarendon Fund (SM), and a Junior Research Fellowship from Kellogg College, University of Oxford (MIA) for support. We thank E Flashman (Department of Chemistry, University of Oxford) for assistance with the $^{18}O_2$ experiment and K Connolly (Institute of Cancer and Genomics Sciences, University of Birmingham) for *Drosophila* cDNA.

References

1. Markolovic S, Wilkins SE, Schofield CJ. Protein hydroxylation catalyzed by 2-oxoglutarate-dependent oxygenases. J Biol Chem. 2015; 290:20712–20722. [PubMed: 26152730]
2. Ploumakis A, Coleman ML. OH, the places you'll go! Hydroxylation, gene expression, and cancer. Mol Cell. 2015; 58:729–741. [PubMed: 26046647]
3. Semenza GL. Oxygen sensing, hypoxia-inducible factors, and disease pathophysiology. Annu Rev Pathol. 2014; 9:47–71. [PubMed: 23937437]
4. Elkins JM, et al. Structure of factor-inhibiting hypoxia-inducible factor (HIF) reveals mechanism of oxidative modification of HIF-1α. J Biol Chem. 2003; 278:1802–1806. [PubMed: 12446723]
5. Walport LJ, Hopkinson RJ, Schofield CJ. Mechanisms of human histone and nucleic acid demethylases. Curr Opin Chem Biol. 2012; 16:525–534. [PubMed: 23063108]
6. Johansson C, et al. The roles of Jumonji-type oxygenases in human disease. Epigenomics. 2014; 6:89–120. [PubMed: 24579949]
7. Morera L, Lübbert M, Jung M. Targeting histone methyltransferases and demethylases in clinical trials for cancer therapy. Clin Epigenetics. 2016; 8:57. [PubMed: 27222667]
8. Chan MC, Holt-Martyn JP, Schofield CJ, Ratcliffe PJ. Pharmacological targeting of the HIF hydroxylases – A new field in medicine development. Mol Aspects Med. 2016; 47–48:54–75. [PubMed: 26791432]

9. Cockman ME, Webb JD, Ratcliffe PJ. FIH-dependent asparaginyl hydroxylation of ankyrin repeat domain-containing proteins. Ann N Y Acad Sci. 2009; 1177:9–18. [PubMed: 19845602]
10. Webby CJ, et al. Jmjd6 catalyses lysyl-hydroxylation of U2AF65, a protein associated with RNA splicing. Science. 2009; 325:90–93. [PubMed: 19574390]
11. Chowdhury R, et al. Ribosomal oxygenases are structurally conserved from prokaryotes to humans. Nature. 2014; 510:422–426. [PubMed: 24814345]
12. Ge W, et al. Oxygenase-catalyzed ribosome hydroxylation occurs in prokaryotes and humans. Nat Chem Biol. 2012; 8:960–962. [PubMed: 23103944]
13. Kato M, et al. Crystal structure of a novel JmjC-domain-containing protein, TYW5, involved in tRNA modification. Nucleic Acids Res. 2011; 39:1576–1585. [PubMed: 20972222]
14. Feng T, et al. Optimal translational termination requires C4 lysyl hydroxylation of eRF1. Mol Cell. 2014; 53:645–654. [PubMed: 24486019]
15. Zhuang Q, Feng T, Coleman ML. Modifying the maker: Oxygenases target ribosome biology. Transl. 2015; 3:e1009331.
16. Del Rizzo PA, Krishnan S, Trievel RC. Crystal structure and functional analysis of JMJD5 indicate an alternate specificity and function. Mol Cell Biol. 2012; 32:4044–4052. [PubMed: 22851697]
17. Markolovic S, et al. Structure-function relationships of human JmjC oxygenases—demethylases versus hydroxylases. Curr Opin Struct Biol. 2016; 41:62–72. [PubMed: 27309310]
18. Rose NR, McDonough MA, King ONF, Kawamura A, Schofield CJ. Inhibition of 2-oxoglutarate dependent oxygenases. Chem Soc Rev. 2011; 40:4364–4397. [PubMed: 21390379]
19. Kandoth C, et al. Integrated genomic characterization of endometrial carcinoma. Nature. 2013; 497:67–73. [PubMed: 23636398]
20. Matsunami N, et al. Identification of rare DNA sequence variants in high-risk autism families and their prevalence in a large case/control population. Mol Autism. 2014; 5:5. [PubMed: 24467814]
21. Lancaster DE, et al. Disruption of dimerization and substrate phosphorylation inhibit factor inhibiting hypoxia-inducible factor (FIH) activity. Biochem J. 2004; 383:429–437. [PubMed: 15239670]
22. Ishikawa K, Azuma S, Ikawa S, Semba K, Inoue JI. Identification of DRG family regulatory proteins (DFRPs): Specific regulation of DRG1 and DRG2. Genes to Cells. 2005; 10:139–150. [PubMed: 15676025]
23. Francis SM, Gas M-E, Daugeron M-C, Bravo J, Seraphin B. Rbg1-Tma46 dimer structure reveals new functional domains and their role in polysome recruitment. Nucleic Acids Res. 2012; 40:11100–11114. [PubMed: 23002146]
24. Mantri M, et al. The 2-oxoglutarate-dependent oxygenase JMJD6 catalyses oxidation of lysine residues to give 5S-hydroxylysine residues. ChemBioChem. 2011; 12:531–534. [PubMed: 22238144]
25. Witkop B. The application of Hudson's lactone rule to γ- and δ-hydroxyamino acids and the question of the configuration of δ-hydroxy-L-lysine from collagen. Experientia. 1956; XII:372–374.
26. Myllyharju J, Kivirikko KI. Collagens and collagen-related diseases. Ann Med. 2001; 33:7–21. [PubMed: 11310942]
27. Leśniak RK, Markolovic S, Tars K, Schofield CJ. Human carnitine biosynthesis proceeds via (2*S*, 3*S*)-3-hydroxy-N^{ϵ}-trimethyllysine. Chem Commun. 2017; 53:440–442.
28. Daugeron M-C, Prouteau M, Lacroute F, Séraphin B. The highly conserved eukaryotic DRG factors are required for efficient translation in a manner redundant with the putative RNA helicase Slh1. Nucleic Acids Res. 2011; 39:2221–2233. [PubMed: 21076151]
29. Ishikawa K, et al. Cloning and characterization of Xenopus laevis drg2, a member of the developmentally regulated GTP-binding protein subfamily. Gene. 2003; 322:105–112. [PubMed: 14644502]
30. Yang M, et al. Factor-inhibiting hypoxia-inducible factor (FIH) catalyses the post-translational hydroxylation of histidinyl residues within ankyrin repeat domains. FEBS J. 2011; 278:1086–1097. [PubMed: 21251231]

31. Klose RJ, Kallin EM, Zhang Y. JmjC-domain-containing proteins and histone demethylation. Nat Rev Genet. 2006; 7:715–727. [PubMed: 16983801]
32. Walport LJ, et al. Arginine demethylation is catalysed by a subset of JmjC histone lysine demethylases. Nat Commun. 2016; 7:11974. [PubMed: 27337104]
33. Mantri M, Zhang Z, McDonough MA, Schofield CJ. Autocatalysed oxidative modifications to 2-oxoglutarate dependent oxygenases. FEBS J. 2012; 279:1563–1575. [PubMed: 22251775]
34. Matheisl S, Berninghausen O, Becker T, Beckmann R. Structure of a human translation termination complex. Nucleic Acids Res. 2015; 43:8615–8626. [PubMed: 26384426]
35. Brown A, Shao S, Murray J, Hegde RS, Ramakrishnan V. Structural basis for stop codon recognition in eukaryotes. Nature. 2015; 524:493–496. [PubMed: 26245381]
36. Powers JC, Asgian JL, Ekici OD, James KE. Irreversible inhibitors of serine, cysteine, and threonine proteases. Chem Rev. 2002; 102:4639–4750. [PubMed: 12475205]
37. Nelson BJ, Maas KJ, Dekeyser JL, Stafstrom JP. Association of DRG1 and DRG2 with ribosomes from pea, arabidopsis, and yeast. Int J Plant Sci. 2009; 170:834–844.
38. Ishikawa K, Akiyama T, Ito K, Semba K, Inoue J. Independent stabilizations of polysomal Drg1/Dfrp1 complex and non-polysomal Drg2/Dfrp2 complex in mammalian cells. Biochem Biophys Res Commun. 2009; 390:552–556. [PubMed: 19819225]
39. Leipe DD, Wolf YI, Koonin EV, Aravind L. Classification and evolution of P-loop GTPases and related ATPases. J Mol Biol. 2002; 317:41–72. [PubMed: 11916378]
40. Scotti JS, et al. Human oxygen sensing may have origins in prokaryotic elongation factor Tu prolyl-hydroxylation. Proc Natl Acad Sci. 2014; 111:13331–13336. [PubMed: 25197067]
41. 2-Oxoglutarate-dependent oxygenases. RSC Metallobiology Series No. 3. Royal Society of Chemistry; 2015.
42. Jang SH, Kim A-R, Park N-H, Park JW, Han I-S. DRG2 regulates G2/M progression via the cyclin B1-Cdk1 complex. Mol Cells. 2016; 39:699–704. [PubMed: 27669826]
43. Lu L, Lv Y, Dong J, Hu S, Peng R. DRG1 is a potential oncogene in lung adenocarcinoma and promotes tumor progression via spindle checkpoint signaling regulation. Oncotarget. 2016; 7:72795–72806. [PubMed: 27626498]
44. Wei D, et al. Molecular cloning and expression of two closely related GTP-binding proteins from zebrafish. DNA Seq. 2004; 15:246–250. [PubMed: 15620211]
45. Vlangos CN, Das P, Patel PI, Elsea SH. Assignment of developmentally regulated GTP-binding protein (DRG2) to human chromosome band 17p11.2 with somatic cell hybrids and localization to the Smith-Magenis syndrome critical interval. Cytogenet Cell Genet. 2000; 88:283–285. [PubMed: 10828610]
46. de Krom M, et al. A common variant in DRD3 receptor is associated with autism spectrum disorder. Biol Psychiatry. 2009; 65:625–630. [PubMed: 19058789]
47. de Ligt J, et al. Diagnostic exome sequencing in persons with severe intellectual disability. N Engl J Med. 2012; 367:1921–1929. [PubMed: 23033978]
48. Katz MJ, et al. Sudestada1, a Drosophila ribosomal prolyl-hydroxylase required for mRNA translation, cell homeostasis, and organ growth. Proc Natl Acad Sci. 2014; 111:4025–4030. [PubMed: 24550463]
49. Fischer R, et al. Discovery of candidate serum proteomic and metabolomic biomarkers in ankylosing spondylitis. Mol Cell Proteomics. 2012; 11:M111.013904. [PubMed: 21997733]
50. Xu D, et al. Novel MMP-9 substrates in cancer cells revealed by a label-free quantitative proteomics approach. Mol Cell Proteomics. 2008; 7:2215–2228. [PubMed: 18596065]
51. Pérez-Arellano I, Spínola-Amilibia M, Bravo J. Human Drg1 is a potassium-dependent GTPase enhanced by Lerepo4. FEBS J. 2013; 280:3647–57. [PubMed: 23711155]
52. Gault J, et al. High-resolution mass spectrometry of small molecules bound to membrane proteins. Nat Methods. 2016; 13:333–336. [PubMed: 26901650]
53. Parsons TB, et al. Optimal synthetic glycosylation of a therapeutic antibody. Angew Chemie Int Ed. 2016; 55:2361–2367.
54. Otwinowski Z, Minor W. Processing of X-ray diffraction data collected in oscillation mode. Methods Enzymol. 1997; 276:307–326.

55. Adams PD, et al. PHENIX: a comprehensive Python-based system for macromolecular structure solution. Acta Crystallogr D Biol Crystallogr. 2010; 66:213–221. [PubMed: 20124702]
56. McCoy AJ, et al. Phaser crystallographic software. J Appl Crystallogr. 2007; 40:658–674. [PubMed: 19461840]
57. Smart OS, et al. Exploiting structure similarity in refinement: automated NCS and target-structure restraints in BUSTER. Acta Crystallogr D Biol Crystallogr. 2012; 68:368–380. [PubMed: 22505257]
58. Brünger AT, et al. Crystallography & NMR system: A new software suite for macromolecular structure determination. Acta Crystallogr D Biol Crystallogr. 1998; 54:905–921. [PubMed: 9757107]
59. Emsley P, Cowtan K. Coot: Model-building tools for molecular graphics. Acta Crystallogr D Biol Crystallogr. 2004; 60:2126–2132. [PubMed: 15572765]
60. Chen VB, et al. MolProbity: all-atom structure validation for macromolecular crystallography. Acta Crystallogr D Biol Crystallogr. 2010; 66:12–21. [PubMed: 20057044]

Europe PMC Funders Author Manuscripts

Europe PMC Funders Author Manuscripts

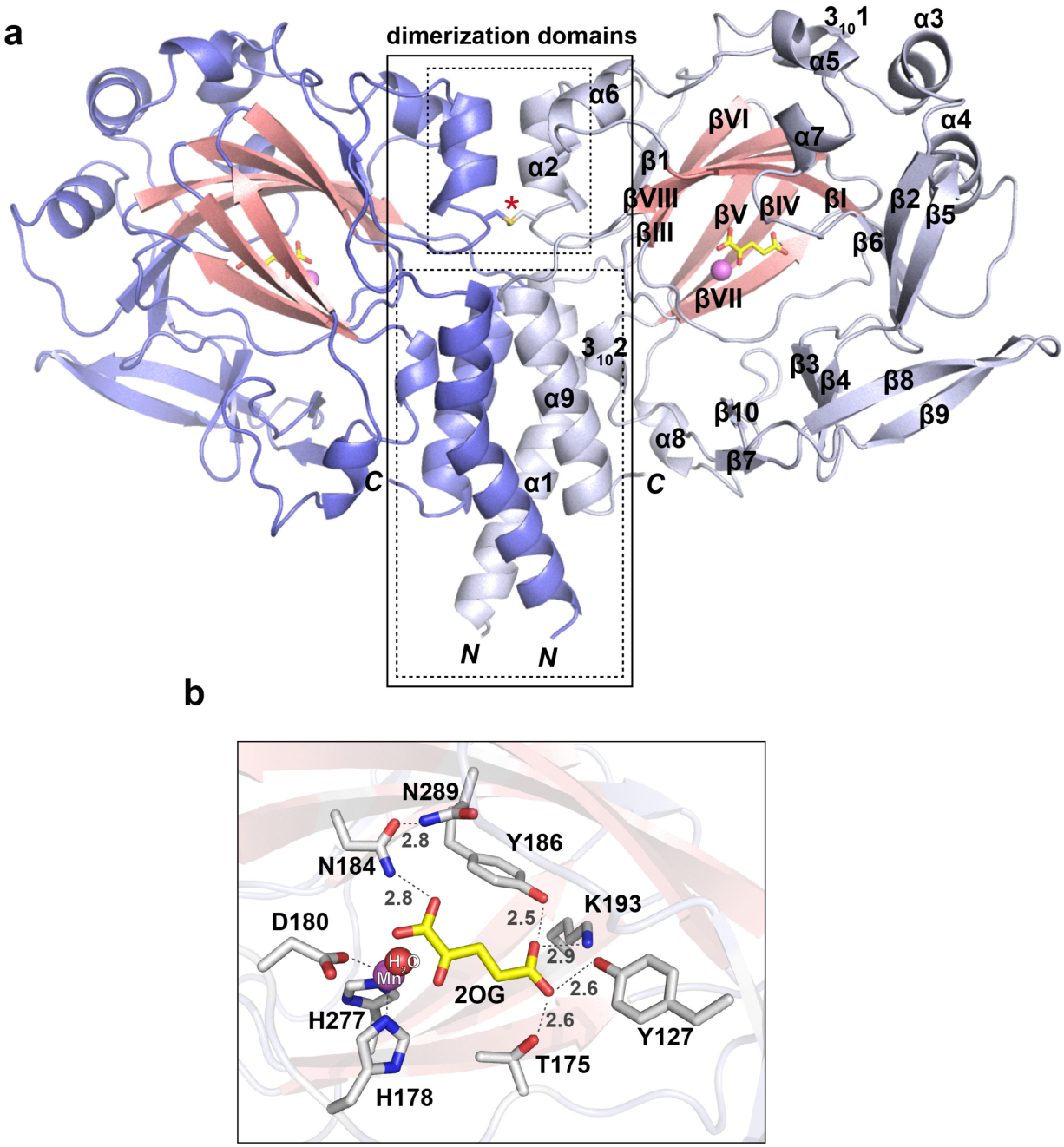

Figure 1. Structural analyses of the JmjC hydroxylase, JMJD7.

(**a**) View from a crystal structure of human JMJD7 complexed with Mn(II) (violet sphere) and 2OG (yellow) showing the unique dimerization interface, which involves regions both *N*- and *C*-terminal to the double-stranded β-helix (DSBH) core fold and the disulfide between Cys47 of each monomer (*, red). β-Strands comprising the distorted 8-stranded (I-VIII) DSBH, conserved in 2OG oxygenases, are in salmon. (**b**) At the active site, Mn (substituting for Fe(II), violet sphere) is octahedrally coordinated by H178, D180, H277, the 2OG oxalyl group (yellow), and water (red sphere). 2OG is apparently tightly bound by

hydrogen bonding/electrostatic interactions between its C5 carboxylate and Y127, T175, Y186, and K193, and its C1 carboxylate with N184 and N289 (dotted lines, numerical values represent H-bond distances in Å).

Europe PMC Funders Author Manuscripts

Europe PMC Funders Author Manuscripts

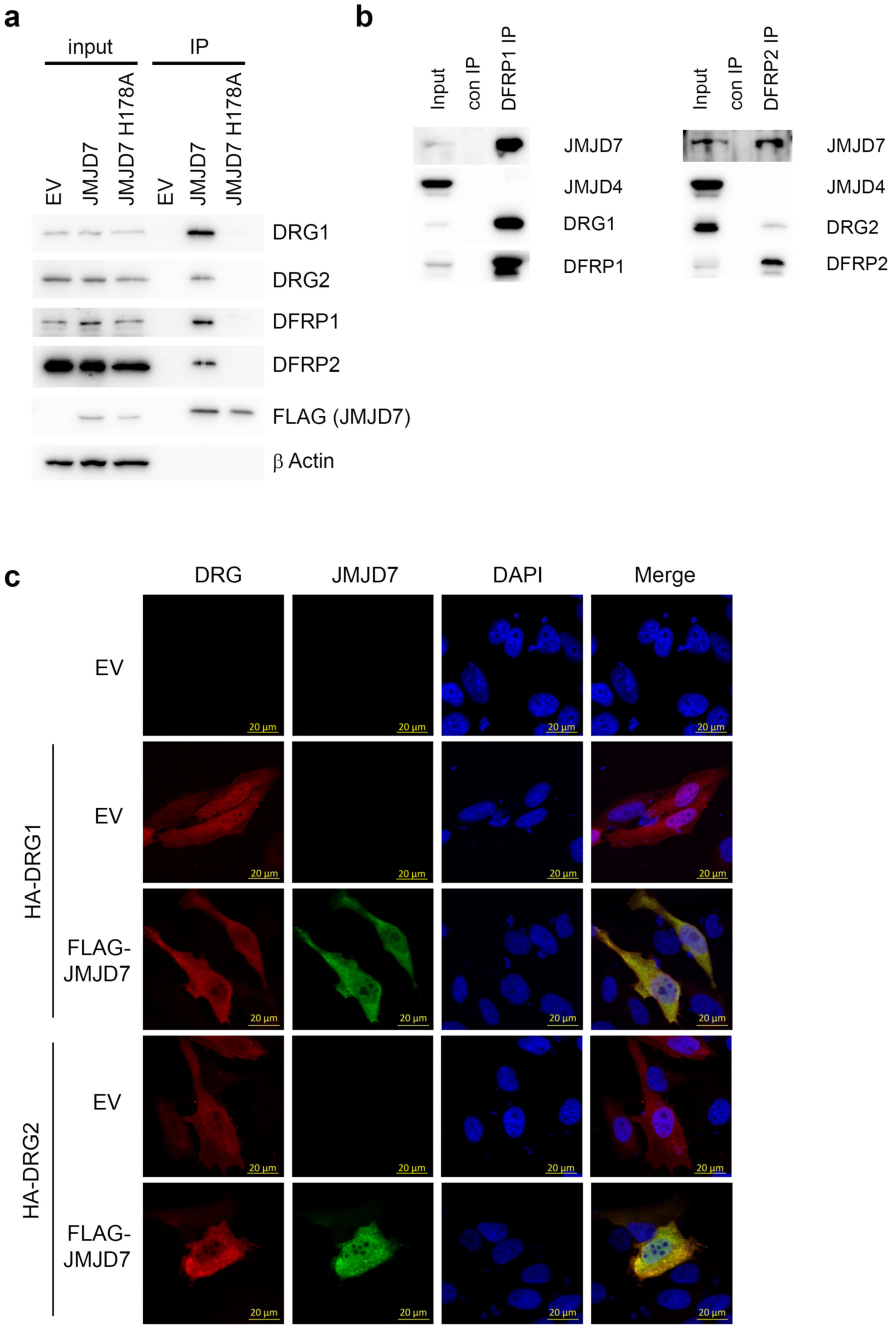

Figure 2. JMJD7 interacts with DRG/DFRP complexes in an active site dependent manner.

(**a**) Interaction of JMJD7 and DRG/DFRP is consistent with proteomic analyses (Supplementary Fig. 9a). 3x-FLAG wildtype or inactive (H178A) JMJD7 were produced in doxycycline-inducible HEK293T cells before anti-FLAG immunopurification (IP) and western blotting with the indicated antibodies. Note the lack of interaction of DRG and DFRP proteins with JMJD7 H178A. The specificity of endogenous DRG antibodies was verified by siRNA knockdown (Supplementary Fig. 9f). Immunoprecipitation experiments validating proteomic data were repeated three times, with similar results. Uncropped western

blots are provided in Supplementary Figure 27. (**b**) Endogenous DRG/DFRP complexes contain endogenous JMJD7. Endogenous DFRP1 (left) or DFRP2 (right) complexes were immunopurified from HEK293T cells prior to western blotting with the indicated antibodies. Note that immunoprecipitation samples were diluted 1:10 prior to analyses of 'bait' (DFRP/DRG levels). This interaction experiment was repeated three times, with similar results. Uncropped western blots are provided in Supplementary Figure 28. (**c**) Co-localization of DRG1/2 and JMJD7. HeLa cells were transfected with control (empty vector, EV), FLAG-JMJD7 and/or HA-DRG1/2 prior to immunostaining for HA (red) and JMJD7 (green) and labeling nuclei with DAPI. This experiment was repeated three times, with similar results.

Europe PMC Funders Author Manuscripts

Europe PMC Funders Author Manuscripts

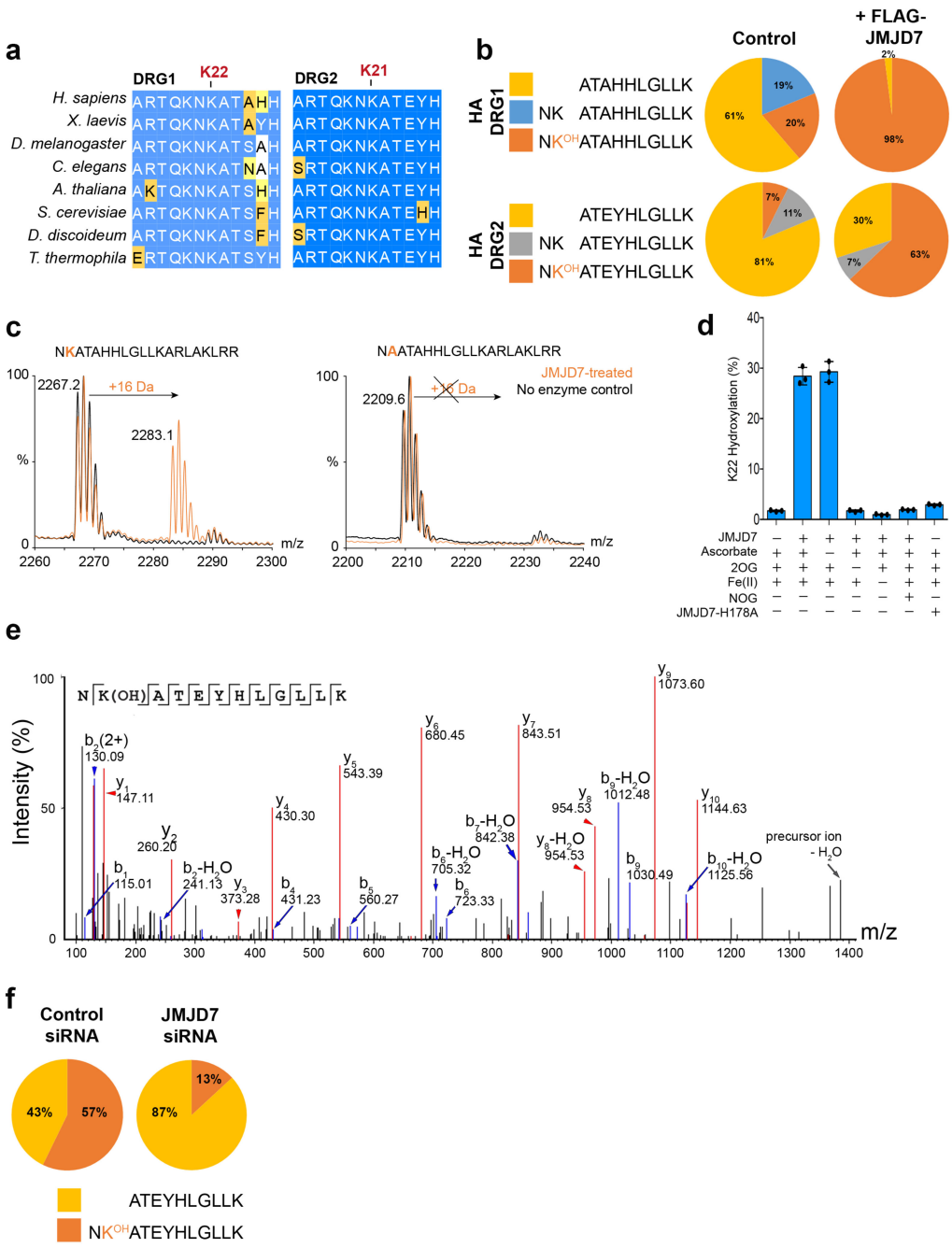

Figure 3. JMJD7 catalyzes lysyl-hydroxylation of the DRG1/2 GTPases.

(**a**) Alignment of the conserved DRG1/2 sequences hydroxylated by JMJD7 in different eukaryotes (Protein BLAST; figure was made using Clustal Omega and GeneDoc). (**b**) Qualitative analysis of the extent of (upper) DRG1 K22 and (lower) DRG2 K21 hydroxylation in the (left) absence or (right) presence of JMJD7 overexpression. Trypsinolysis at K22 of DRG1 and K21 of DRG2 is impeded by hydroxylation, complicating quantification: precursor signal intensities of the indicated tryptic fragments, as judged by precursor ion chromatogram analysis, were used; a shift in proportion of the fully-

Europe PMC Funders Author Manuscripts

trypsinized peptide signal to the uncleaved trypsinized lysyl-hydroxylated peptide signal is indicative of increased hydroxylation. See Supplementary Fig. 10 for MS/MS fragments detected. (**c**) Representative MALDI mass spectra for (left) wildtype $DRG1_{21-40}$ and (right) K22A $DRG1_{21-40}$ in the absence (black) or presence (orange) of JMJD7. The K22A substitution nearly ablates peptide hydroxylation. This experiment was repeated three times, with similar results. (**d**) Representative MALDI-MS assays with $DRG1_{16-40}$ in presence/absence of co-factors/substrates and inhibitor. Ascorbate has no effect on JMJD7 activity in the linear range (the activity of some 2OG oxygenases is promoted by ascorbate18). The JMJD7-H178A mutant has reduced activity. Data represent the mean ± standard deviation (n = 3 replicates with a single biological sample) after incubation for 5 min at 37°C. This assay was repeated twice, with similar results. (**e**) MS/MS spectra of the K21 hydroxylated tryptic peptide fragment from endogenous DRG2 (see Supplementary Fig17a-c for extended data, and Supplementary Fig. 17d-f for DRG1). Note that fragments of the hydroxylated peptide lose water (-18 Da, likely to give a C2/C3 dehydro- species, consistent with C3 hydroxylation), so most b-ions appear as pairs. Similar spectra were identified in multiple samples from two independent experiments. (**f**) Quantification of endogenous DRG2 K21 hydroxylation following control or JMJD7 siRNA. This experiment was repeated twice, with similar results.

Europe PMC Funders Author Manuscripts

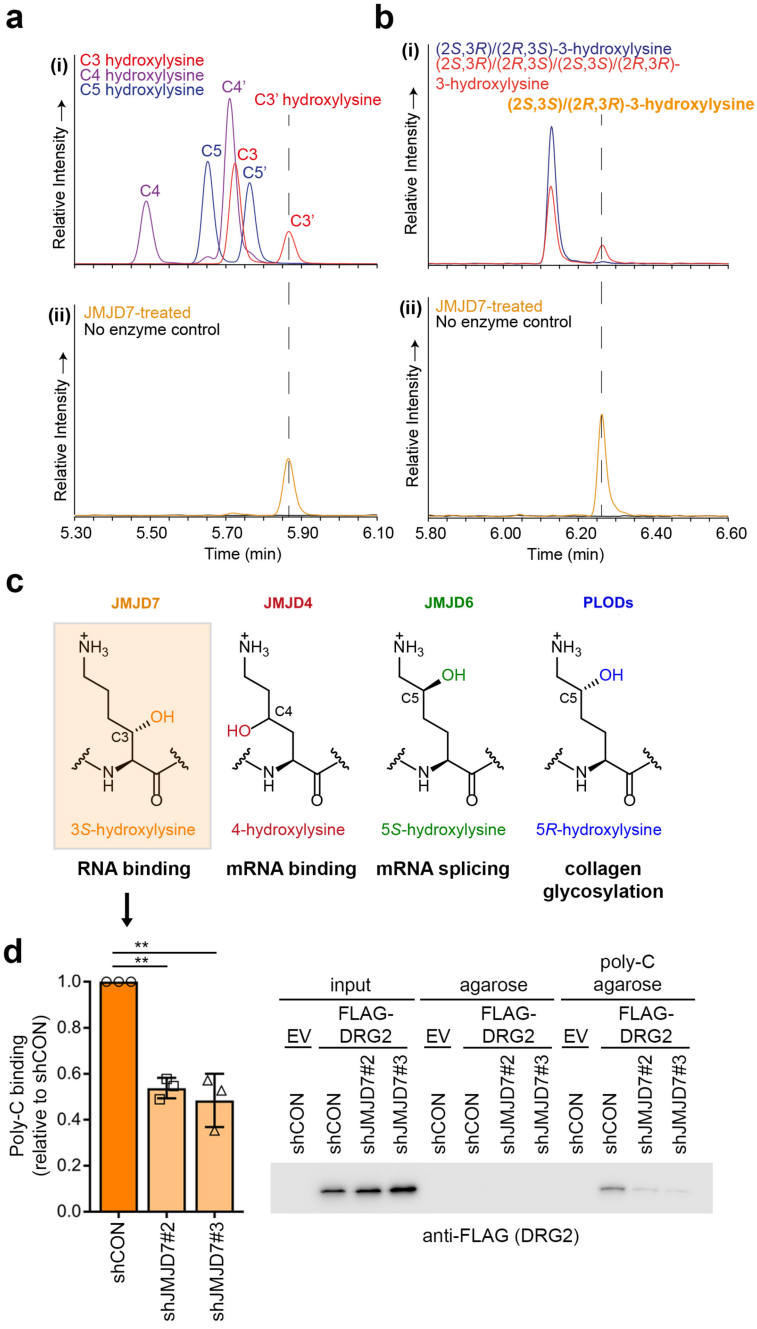

Figure 4. JMJD7 is a (3*S*)-lysyl hydroxylase that promotes DRG ribonucleic acid binding.

(**a**) Overlaid extracted ion chromatograms (XIC; m/z = 503.2) corresponding to: (**i**) C3 (dark blue), C4 (light blue), and C5 (cyan) hydroxylysine standards post-derivatization (two peaks are observed because each standard is a mixture of stereoisomers - (2*S*,X*R*)/(2*R*,X*S*) and (2*S*,X*S*)/(2*R*,X*R*); X is the hydroxylation site, see Supplementary Fig. 19); (**ii**) hydrolyzed DRG1$_{21\text{-}40}$ peptide incubated with (orange) or without (black) JMJD7 prior to hydrolysis. The new product in the JMJD7-treated sample (orange) elutes at the same retention time as one of the C3 stereoisomeric pairs (C3'). (**b**) Overlaid XIC (m/z = 503.2) corresponding to:

(**i**) C3 hydroxylysine standard sample (dark blue) and (2*S*,3*R*)/(2*R*,3*S*)-3-hydroxylysine standard (red) indicates the (2*S*,3*R*)/(2*R*,3*S*)-3-hydroxylysine enantiomeric pair co-elutes with the first peak of the C3 standard; (**ii**) hydrolyzed $DRG1_{21\text{-}40}$ peptide incubated with (orange) or without (black) JMJD7. The new peak in JMJD7-sample (orange) elutes at the same retention time as the standard corresponding to (2*S*,3*S*)/(2*R*,3*R*)-3-hydroxylysine (see Supplementary Fig. 19). Amino acid analyses were repeated two or three times, with similar results. (**c**) Currently described forms of lysyl hydroxylation and their functions. (**d**) JMJD7 knockdown reduces the affinity of purified DRG2 for an RNA poly-C (cytidine nucleotide) agarose column. 3x-FLAG DRG2 was purified from doxycycline-inducible control shRNA cells (shCON) or two independent JMJD7 shRNA cell lines (#2 and #3) before anti-FLAG purification and incubation with poly-C agarose. Captured FLAG-DRG2 was detected by anti-FLAG western blotting (right; uncropped western blots are provided in Supplementary Figure 39) and quantified in three independent experiments, with similar results (left): Data represent the mean ± s.e.m. (n=3 biologically independent experiments) analyzed by 2-sided students t-test (** $P<0.01$; $P=0.0016$ shJMJD7#2 and 0.0082 shJMJD7#3).

Europe PMC Funders Author Manuscripts